Toward Efficient and Omnidirectional n-Type Si Solar Cells: Concurrent Improvement in Optical and Electrical Characteristics by Employing Microscale Hierarchical Structures

Hsin-Ping Wang,[†,‡,#] Tzu-Yin Lin,[†,#] Meng-Lin Tsai,[†] Wei-Chen Tu,[†] Ming-Yi Huang,[§] Chee-Wee Liu,[†] Yu-Lun Chueh,[‡,*] and Jr-Hau He[†,*]

[†]Institute of Photonics and Optoelectronics and Department of Electrical Engineering, National Taiwan University, Taipei 10617, Taiwan, Republic of China, [‡]Department of Materials Science and Engineering, National Tsing Hua University, Hsinchu 30013, Taiwan, Republic of China, and [§]Advanced Technology Department, AU Optronic Corporation, Taichung, Taiwan, Republic of China. [#]H.-P. Wang and T.-Y. Lin contributed equally to this work.

ABSTRACT We demonstrated that hierarchical structures combining different scales (*i.e.*, pyramids from 1.5 to 7.5 μm in width on grooves from 40 to 50 μm in diameter) exhibit excellent broadband and omnidirectional light-trapping characteristics. These microscaled hierarchical structures could not only improve light absorption but prevent poor electrical properties typically observed from nanostructures (*e.g.*, ultra-high-density surface defects and nonconformal deposition of following layers, causing low open-circuit voltages and fill factors). The microscaled hierarchical Si heterojunction solar cells fabricated with hydrogenated amorphous Si layers on as-cut Czochralski n-type substrates show a high short-circuit current density of 36.4 mA/cm^2, an open-circuit voltage of 607 mV, and a conversion efficiency of 15.2% due to excellent antireflection and light-scattering characteristics without sacrificing minority carrier lifetimes. Compared to cells with grooved structures, hierarchical heterojunction solar cells exhibit a daily power density enhancement (69%) much higher than the power density enhancement at normal angle of incidence (49%), demonstrating omnidirectional photovoltaic characteristics of hierarchical structures. Such a concept of hierarchical structures simultaneously improving light absorption and photocarrier collection efficiency opens avenues for developing large-area and cost-effective solar energy devices in the industry.

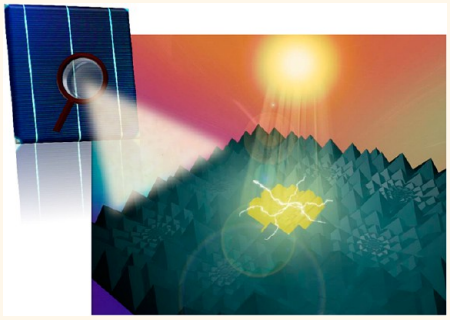

KEYWORDS: Si heterojunction solar cells · microscaled hierarchical structure · light-scattering · omnidirectional n-type Si solar cells

Light absorption in photovoltaic (PV) devices has become critical with continuous improvements in cell design *via* coupling light as much as possible into cells for boosting cell efficiency. Therefore, a lot of research efforts have focused on photon management techniques to precisely control and enhance the light−matter interaction at the active layer. In the past decade, nanowire (NW) structures have attracted exceptional attention in either optical enhancements or electrical improvements for PV applications due to their unique architectures.[1] From the optical viewpoint, NWs significantly suppress the reflection in wide ranges of wavelengths and angles of incidence (AOIs) *via* improving the impedance matching at the interface of air and devices.[2−4] From the electrical viewpoint, photocarriers can easily diffuse to the p−n junction interface along the radial direction and be effectively extracted *via* radial p−n junction design. Moreover, high surface areas of NWs provide large junction areas, increasing the amount of collected photocarriers.[5,6] However, the increased amount of photons entering the structures cannot be efficiently confined in the active layer to further enhance light absorption due to less interaction between nanoscaled surfaces of NW structures and incident light. High-density defect states caused by ultrahigh aspect ratio and the nanoscaled rough surface of NWs would result in a high

* Address correspondence to jhhe@cc.ee.ntu.edu.tw; ylchueh@mx.nthu.edu.tw.

Received for review January 15, 2014 and accepted February 18, 2014.

Published online February 18, 2014
10.1021/nn500257g

recombination rate. Furthermore, the high aspect ratio of NWs also leads to poor coverage of following layers or electrodes. Thus, the expected boosted short-circuit current density (J_{SC}) is partially counterbalanced by poor open-circuit voltages (V_{OC}) and fill factors (FF). The performance of such nanostructured solar cells may not be improved or even become worse. Therefore, it is imperative to develop new ways to break through the difficult situation for boosting cell performance.

The creation of hierarchical architectures that combine materials of different classes, electrical/optical properties, and scales to provide synergistic and tailorable performance has attracted a great deal of attention.[7−14] For example, Hsu *et al*. reported integrating carbon nanotubes and TiO_2 shells with radial Schottky barriers in a core−shell fashion for breaking the compromise between the photogain and the response/recovery speed of NW photodetectors.[11] As for the application in photon management, the hierarchical structure provides a hybrid concept creating two-scale structures to optimize PV performance and is expected to replace pure NW structures for solar applications.[5,12−14] For example, Si microgrooves and ZnO NWs were employed on monocrystalline Si solar cells for eliminating the reflection loss.[14] Fan *et al*. developed three-dimensional hierarchical nanorod arrays with greatly enhanced light absorption.[7] How to design the cells not only to absorb light effectively but also to extract photocarriers efficiently with minimal loss is one of the most important issues for putting structured solar cells into practice.

It is known that the AOI of the sun changes during the day. Moreover, after sunlight passes through the atmosphere and reaches the earth, it contains a large amount of scattered (diffused) light. On cloudy days, over 90% of the light is diffused. However, for polished Si surfaces, nearly 40% of light is reflected when averaged over all AOIs and the solar spectrum.[15] Conventional Si cells with micropyramidal structures also show insufficient light trapping during the day because the reflection is angular dependent due to the pyramidal architecture. Therefore, it is critical to develop structures with omnidirectional light-harvesting characteristics to replace conventional micropyramidal structures. Additionally, as expensive sun-tracking and concentrator systems make their way into high-efficiency PV applications, most tracking and concentrator systems are specified for direct radiation only, which means that these tracking systems work well on bright, clear days but poorly on hazy days. More importantly, additional expensive tracking systems might not be workable for cost-effective solar cells. Accordingly, the new optical requirement for solar cells, omnidirectional PV performance, emerges for reducing wasted solar energy caused by the angular effect. With better omnidirectional PV performance, more daily generation power would be expected. To date, most studies in photon management only report omnidirectional light-harvesting optical effects,[16,17] but few works readily realize omnidirectional solar cells in practice.[5,18−20]

While the p-type Si substrate is a more common PV material (for example, 84% of the PV module production in 2011), a world-record high efficiency of 24.7% utilizing Panasonic's Si heterojunction (SHJ) with intrinsic thin-layer technology among all kinds of Si-based solar cells was achieved with a 98 μm thick Czochralski (CZ) n-type monocrystalline Si cell in 2013.[21] The driving force for the development of n-type Si solar cells is based on the inherent disadvantages of p-type Si, *i.e*., the severe light-induced degradation caused by the presence of boron and oxygen in the wafers[22] and the high sensitivity to impurities, such as iron, that are usually present in the Si feedstock.[23] As a consequence, there is a growing interest for the past years in the scientific research and the industrial implementation of n-type Si-based PV technologies with photon management by structuring Si substrates, which is summarized in Table S1 in the Supporting Information.

In this study, the photon management has been employed with Si hierarchical structures combining different scales (*i.e*., pyramids from 1.5 to 7.5 μm in width on grooves from 40 to 50 μm in diameter) *via* isotropic wet etching followed by anisotropic wet etching. The most efficient light-trapping structures for achieving high-efficiency solar cells are fabricated by complicated or expensive processes. Maskless wet etching is an alternative to expensive processes. Combining isotropic and anisotropic chemical etching, large-area hierarchical structures can be obtained by cost- and time-effective manufacturing technology. The pyramid/groove hierarchical structures exhibit an average total reflectance (R_{total}) as low as 13.2% from 300 to 1100 nm (as compared to grooved structures (38.3%) and pyramidal structures (17.2%)), and the specular reflectance ($R_{specular}$) is below 2% even at an AOI of up to 75°. The excellent broadband and omnidirectional antireflection (AR) abilities of hierarchical structures result from pyramids arranged at different heights on grooved surfaces, providing more opportunities for the incoming light to undergo multiple bounces and thereby reducing the overall surface reflectance. Moreover, the strong light scattering caused by microscaled hierarchical structures enhances light−matter interactions and thus increases effective optical thickness to increase light absorption in devices. SHJ solar cells fabricated on cost-effective CZ n-type Si with pyramid/groove hierarchical structures exhibit a power conversion efficiency of 15.2% with a J_{SC} of 36.4 mA/cm^2, V_{OC} of 607 mV, and FF of 68.66%, demonstrating a promising photon management scheme to achieve high J_{SC} without compromising V_{OC} and FF. As compared to purely grooved

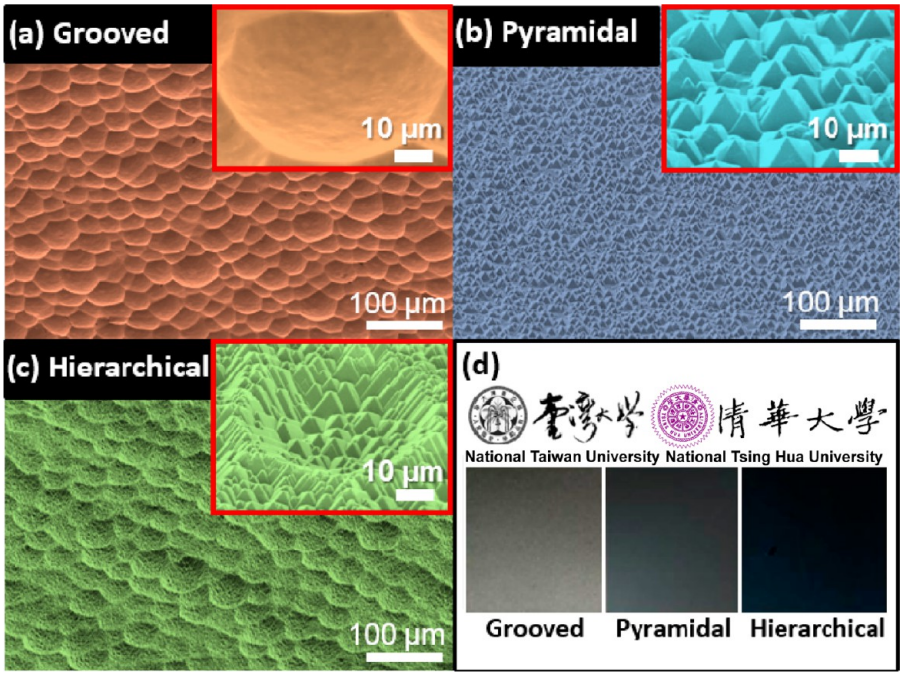

Figure 1. Scanning electron microscopy images of different Si surface structures: (a) grooved, (b) pyramidal, and (c) hierarchical structures. The insets in (a)−(c) are high-magnification images. (d) Photographic image of three kinds of structures on 16 cm^2 wafers.

structures, more pronounced enhancement of the generated power density of SHJ cells with hierarchical surfaces at high AOIs is observed (from 49% at normal AOI to 104% at 60°), leading to a daily power density enhancement of 69%, which demonstrates the excellent omnidirectional characteristics of hierarchical Si surfaces for practical PV applications. Such omnidirectional PV performance using wet-etched hierarchical structures offers an attractive solution for large-area industrial production of bulk monocrystalline/polycrystalline Si, thin film, and organic solar cells.

RESULTS AND DISCUSSION

For large-scale solar cell production, the use of cost-effective CZ Si substrates becomes the only possible option with economic considerations, although float-zoning Si substrates show high carrier lifetimes and thus high efficiencies (in most industry cases).[24] Instead of polished Si fabricated by expensive chemical mechanical polishing processes, the solar cell fabrication directly starting with as-cut Si wafers would save production costs. Accordingly, in this study we use as-cut CZ n-type Si substrates to demonstrate the achievement, and thus polished cells are not shown for comparison. Three kinds of Si surfaces, namely, (i) grooved surfaces, (ii) pyramidal surfaces, and (iii) hierarchical surfaces consisting of different scaled grooves and pyramids, are compared to show the distinguished achievement of hierarchical surfaces in photon management. Moreover, to fairly examine the feasibility of photon management using three kinds of surfaces, only the best light-harvesting results for each surface condition are shown and discussed hereinafter.

After Si substrates were isotropically textured using maskless acidic etching with HF, HNO_3, and H_3PO_4 with 12:1:12 volume ratio percentage concentration for 2 min, grooved surfaces with diameters ranging from 40 to 50 μm and a depth of ~6 μm were formed (Figure 1a). Si oxidation occurred upon exposure to HNO_3, and then the oxidized layer was removed by HF *via* forming H_2SiF_6. H_3PO_4 acts as a catalytic agent to moderate etching rates without affecting the morphology of textured surfaces. The round crater-like features of grooved surfaces result from the fact that the etching reaction starts at the defective sites due to their low activation energy and then diffuses to neighboring regions on saw-damaged surfaces. This mechanism also gives rise to the increase in the diameter of round craters with etching time. Random pyramids ranging from 7 to 12 μm in width were fabricated by dipping as-cut Si substrates in the anisotropic etching solution consisting of KOH, isopropyl alcohol, and H_2O with the volume ratio percentage concentration of 1:1:17 at 85 °C for 20 min, as shown in Figure 1b. Such pyramids are formed by the much higher etching rate in the [100] direction than that in the [111] direction due to the higher atomic density in the (111) plane than that in the (100) plane.[24] To form hierarchical Si surfaces consisting of grooved and pyramidal structures, Si substrates with grooved surfaces were anisotropically etched with KOH solution at 85 °C for 9 min (Figure 1c). As the anisotropic etching time of Si increased to 10 min, the shape of the grooves

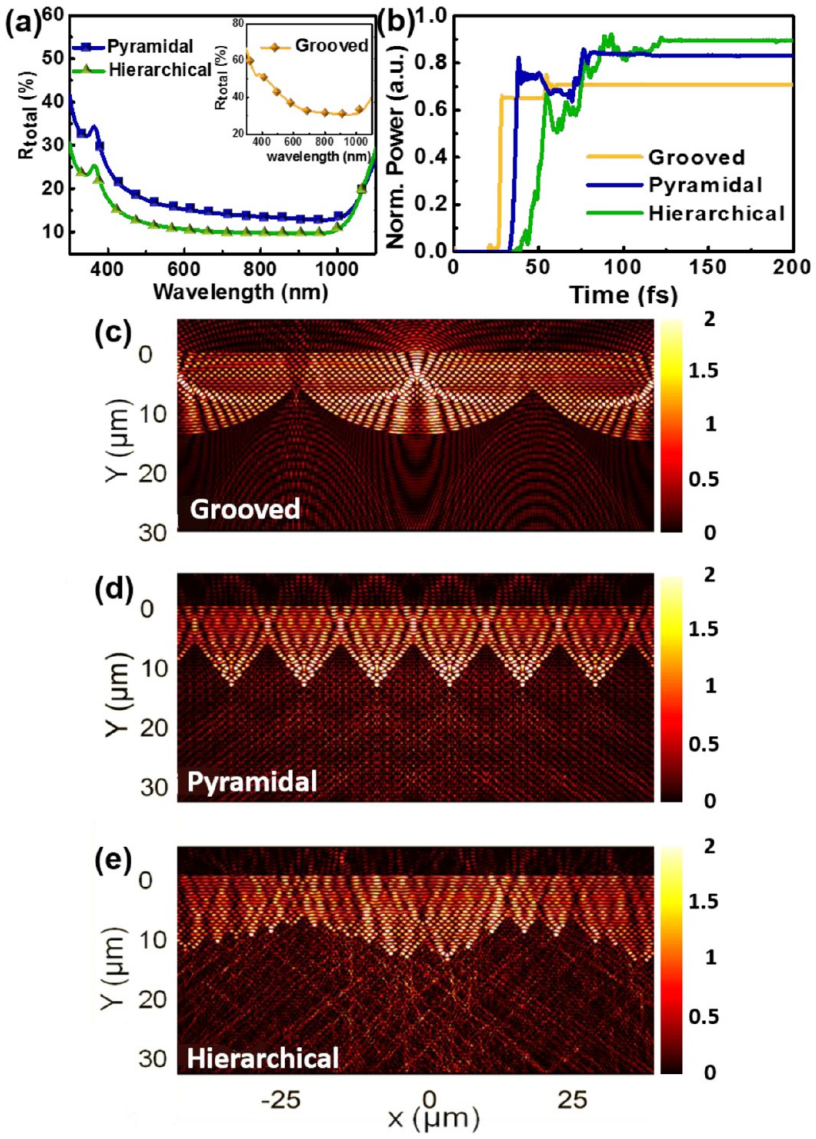

Figure 2. (a) Total reflectance spectra of three kinds of surface structures. Steady-state, normalized electric field (|*E*|) distribution at a wavelength of 550 nm by FDTD simulation with three kinds of Si surface conditions: (b) the normalized optical power detected at *y* = 20 μm (can be found in (c)−(e)) at 550 nm and the corresponding light-propagation images of (c) grooved, (d) pyramidal, and (e) hierarchical structures.

disappeared, leading to an increase in the reflectance (Figure S1 in the Supporting Information). Combining isotropic and anisotropic chemical etching, large-area hierarchical structures can be obtained by cost- and time-effective manufacturing technology. Figure 1d shows the photographic images of three kinds of Si surfaces of 16 cm^2 in size. In the figures, a uniform distribution in color on the entire sample demonstrates the feasibility for industrial production. After chemical wet etching, the thicknesses of substrates with grooved, pyramidal, and hierarchical surfaces are ~100, ~150, and ~100 μm, respectively (Figure S2 in the Supporting Information).

To analyze the light-harvesting characteristics of different surfaces, the R_{total} spectra in the wavelength range from 300 to 1100 nm were measured (Figure 2a). It is observed that grooved surfaces reflect ~38.3% of the incident light on average. This unsatisfactory light-trapping property of the grooved surfaces stems from the wide hemisphere diameter of shallow grooved structures causing the incoming light to be strongly reflected from the surface.[25] Pyramidal surfaces ensure light undergoes multiple reflections on the surface of the cell before being reflected back to the air and thus exhibit a better light-trapping scheme (average R_{total} = 17.2%) than that of grooved surfaces.[26] Hierarchical structures consisting of grooves and pyramids exhibit the lowest reflectance (average 13.2%), although the thickness of a substrate with hierarchical structures is thinner than that of a substrate with pyramidal surfaces, which demonstrates the best light-trapping ability among the three kinds of structures. The pyramids arranged at different heights on grooved surfaces can provide the opportunity for the incoming

light to undergo more bounces, thereby reducing the overall surface reflection and enhancing the amount of light entering the solar materials.[27,28] Moreover, after light enters the devices, the strong light scattering with large scattering angles caused by the microscaled hierarchical structures can further increase the effective optical thickness, resulting in more light−matter interactions and absorption, which will be discussed later.

To further confirm that the traveling light can be trapped among hierarchical structures by the enhanced scattering effect, the optical simulation based on finite-difference time domain (FDTD) can reveal the distribution and strength of the electric field in grooved, pyramidal, and hierarchical structures. The details about simulated structures and optical parameters used in the FDTD simulation are described in Figure S3 in the Supporting Information. The wavelength for all simulations is selected to be 550 nm. Figure 2b shows the normalized steady-state optical power as a function of time with the detector at y = 20 μm (which can be seen in Figure 2c−e, displaying time-averaged electric field intensity distributions, $|E|$, within grooved, pyramidal, and hierarchical structures of Si, respectively). One can see that normalized steady-state power values are 0.68 for grooved, 0.83 for pyramidal, and 0.90 for hierarchical structures at y = 20 μm (Figure 2b). As shown in Figure 2c, the field intensity of grooved structures diverges significantly, reflecting a high optical loss. Compared with pyramidal structures, the $|E|$ in hierarchical structures shows stronger light scattering with larger scattering angles (Figure 2e), leading to longer absorption length and then enhancing the light absorption. Our hierarchical structures can further enhance the light scattering in substrates than pyramidal structures because of the combination of multiple scales and morphologies of structures. The strong scattering effect is an important optical feature of microscaled hierarchical structures for the application of PVs and will be compared with that of nanoscaled hierarchical structures later. Overall, the simulation results indicate that the photon management employing hierarchical structures can increase the number of photons being trapped in the structures, in agreement with the experimental results shown above.

To investigate the omnidirectional light-trapping ability of hierarchical structures, the $R_{specular}$ spectra of grooved, pyramidal, and hierarchical structures at different AOIs were measured and are shown in Figure 3. In general, the omnidirectional light-trapping ability is hierarchical > pyramidal > grooved structures; hierarchical structures with $R_{specular}$ below 2% at all AOIs show excellent broadband and omnidirectional abilities to suppress undesired reflection. The omnidirectional characteristics of hierarchical structures are particularly beneficial for the current Si solar cell

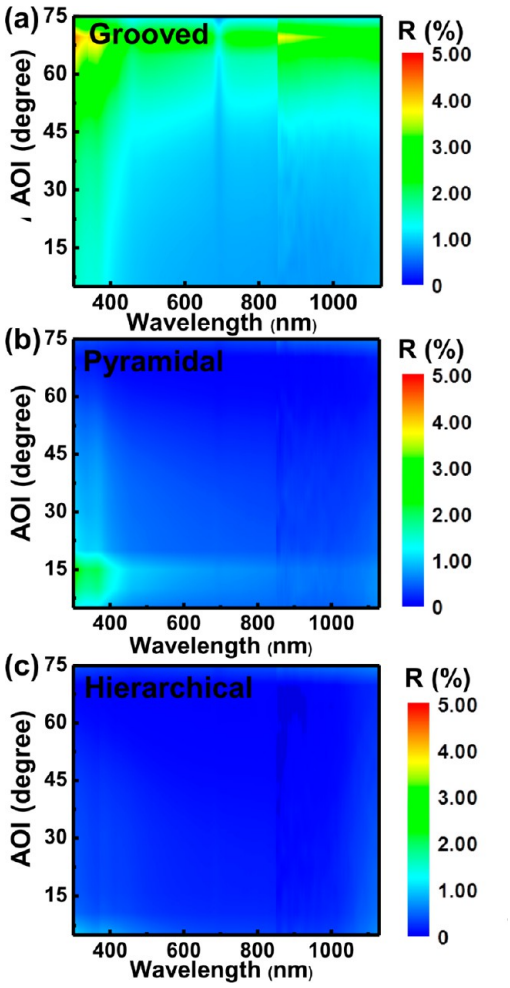

Figure 3. Reflectance spectra as a function of AOI and wavelength on three kinds of Si surface conditions: (a) grooved, (b) pyramidal, and (c) hierarchical structures.

industry, which widely uses angular-dependent pyramids as AR structures. The omnidirectional effects on the practical PV performance will be demonstrated later.

Figure 4 shows the minority carrier lifetime characteristics of three kinds of structures passivated by intrinsic hydrogenated amorphous Si (a-Si:H) layers characterized by the quasi-steady-state photoconductance technique. The grooved structures exhibit the shortest carrier lifetime due to a large amount of (100) planes exposed on the grooved surfaces and the formation of nanoscaled rough surfaces caused by the drastically exothermic reaction during the etching process.[29] The (100) plane exhibits two dangling bonds, while the (111) plane has only one, leading to the fact that the surface state density of the (111) plane is lower than that of the (100) plane.[30−32] Accordingly, during the a-Si:H deposition, the epitaxial Si (epi-Si) layer would be formed more easily on the more defective (100) plane as compared with the (111) plane. The epi-Si is highly defective and thus decreases the surface passivation effect, giving rise to a drop in

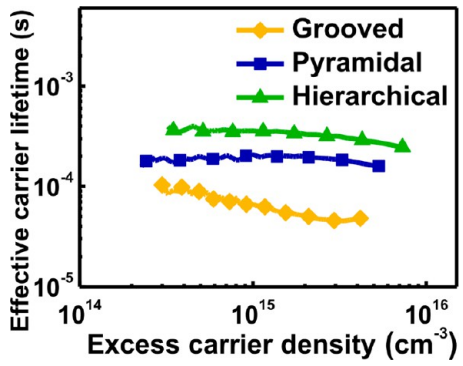

Figure 4. Minority carrier lifetime of three kinds of Si surface structures passivated by intrinsic a-Si:H layers.

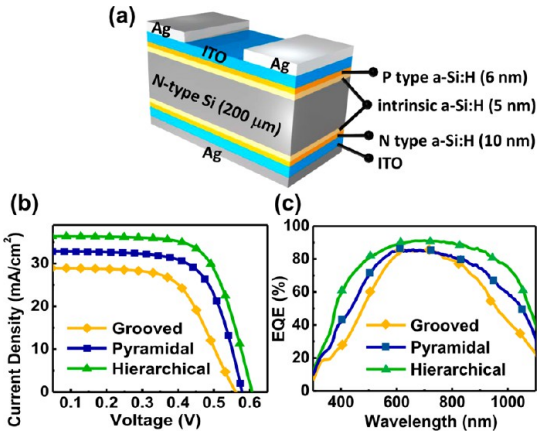

Figure 5. (a) Schematic of SHJ solar cells. (b) *J*−*V* curves and (c) EQEs for SHJ solar cells with grooved, pyramidal, and hierarchical structures.

the effective carrier lifetime and the lowered V_{OC} of solar cells due to a high recombination rate.[33,34] In contrast, pyramidal structures with many (111) planes exposed due to the anisotropic etching nature exhibit a higher minority carrier lifetime. The hierarchical structures, which also expose a large amount of (111) planes on the surface, reach an even higher minority carrier lifetime (217 μs) than pyramidal structures (157 μs). The carrier lifetime difference between pyramidal and hierarchical structures is due to the actual thickness difference of Si substrates after the etching process (Figure S2 in the Supporting Information). The effective carrier lifetime (τ_{eff}) of the total recombination (including surface and bulk recombination) can be expressed as[35]

$$\frac{1}{\tau_{eff}} = \frac{1}{\tau_{bulk}} + \frac{1}{\tau_{surf}} \quad (1)$$

where τ_{bulk} is the bulk lifetime and τ_{surf} is the surface lifetime. Due to the excellent passivation capability of the a-Si:H/monocrystalline Si heterojunction and similar pyramidal surfaces on both pyramidal and hierarchical structures, the τ_{surf} values of pyramidal and hierarchical structures are similar and thus the τ_{bulk} dominates the τ_{eff}. The thickness of substrates with pyramidal structures is ~150 μm after alkaline etching. In contrast, after as-cut substrates are treated with acidic and alkaline etching solutions, the thickness of substrates with hierarchical structures is decreased to ~100 μm. As the wafer thickness is reduced, there is less space available for the bulk recombination, and the edge recombination is suppressed, leading to the increase in the effective lifetime.[36−39] The superior light-harvesting ability of hierarchical structures allows the shrinkage of the thicknesses of PV devices, decreasing the recombination loss. It is worth noting that our microscaled hierarchical structures show the potential to break through the dilemma between optics and electrics for PV devices *via* a meticulous structure design. The surface of microscaled hierarchical structures demonstrated here can be well passivated by the a-Si:H layer deposited by plasma-enhanced chemical vapor deposition processes due to their appropriate microscaled structures and a large number of (111) planes exposed at the surfaces, disregarding the severe surface recombination problem, which is often observed in nanoscaled structures. Hence, substrates with microscaled hierarchical structures showing high effective carrier lifetime (including both τ_{surf} and τ_{bulk}) and excellent light-harvesting ability have great potential for achieving high Jsc, V_{OC}, and FF simultaneously.

To assess the feasibility of photon management using hierarchical structures in practical solar cell applications, SHJ solar cells were fabricated with these structured surfaces. The schematic of SHJ solar cells is displayed in Figure 5a. Plasma-enhanced chemical vapor deposition was carried out at 150 °C for depositing intrinsic a-Si:H layer (5 nm)/p-type a-Si:H layer (6 nm) on the front and intrinsic a-Si:H layer (5 nm)/n-type a-Si:H layer (10 nm) on the rear. The intrinsic a-Si:H provides not only good chemical passivation but also field-effect passivation due to the large band offset existing at the a-Si:H/c-Si interface, minimizing the recombination loss. At the front junction with an intrinsic a-Si:H layer as thin as 5 nm, minority hole carriers are able to tunnel across the intrinsic a-Si:H layer into the p-type a-Si:H layer possibly with some thermal and trap assistance even though the valence band offset is large. The intrinsic a-Si:H layer/n-type a-Si:H layer on the rear provides (i) an excellent rear contact for facilitating majority carrier (electron) transport due to the small conduction band offset and (ii) excellent passivation repelling minority carriers (holes) from the back contact due to the large valence band offset. Note that this excellent band structure design is not achievable in solar cells with p-type Si substrates. Finally, 90 nm thick indium tin oxide (ITO) contacts were deposited on both sides by sputtering, followed by the deposition of Ag grids on the front and a full coverage of Ag on the rear using e-beam evaporation.

The current density−voltage (*J*−*V*) characteristics of the SHJ solar cells with three kinds of surfaces were

TABLE 1. Photovoltaic Parameters of SHJ Solar Cells with Three Kinds of Structures

	J_{SC} (mA/cm^2)	V_{OC} (V)	FF (%)	efficiency (%)
grooved	28.95	0.563	61.77	10.2
pyramidal	32.86	0.580	67.77	12.9
hierarchical	36.36	0.607	68.66	15.2

measured under air mass 1.5 global (AM 1.5G) illumination, as shown in Figure 5b and summarized in Table 1. The SHJ solar cell with grooved structures displays the lowest efficiency of 10.2% with a J_{SC} of 28.95 mA/cm^2 and a V_{OC} of 563 mV resulting from severe optical loss (due to wide-open crater-like surfaces) and high carrier recombination rate (due to highly defective surfaces, confirmed by the minority carrier lifetime measurement shown previously). The cells with pyramidal surfaces with a lot of (111) planes exposed exhibit higher J_{SC} (32.86 mA/cm^2) and V_{OC} (580 mV) due to reduced reflectance and increased minority carrier lifetime. As compared to the SHJ cells with grooved and pyramidal structures, the SHJ cell with hierarchical structures further improves J_{SC} and V_{OC} to 36.36 mA/cm^2 and 607 mV, respectively, leading to the highest efficiency (15.2%), echoing its best light-trapping ability and longest minority carrier lifetime. Moreover, the high efficiency of SHJ solar cells with hierarchical structures can partly be attributed to the FF improvement. The grooved structures with a large number of (100) planes causing epi-Si formation during a-Si:H layer growth may give rise to the poor junction contact, which reflects the high series resistance and the low FF of 61.77%. The pyramid-structured cell with a large number of (111) planes exposed exhibits a FF of 67.77%. For the hierarchical structures with a large number of (111) planes, the thinned wafers caused by acidic and alkaline etching solutions further reduce the series resistance and improve the FF up to 68.66%.

The increase in J_{SC} and V_{OC} partly contributed by improved minority carrier lifetime can be understood by the relations below.

$$V_{OC} = \frac{kT}{q} \ln\left(\frac{\Delta n(N_{D,A} + \Delta n)}{{n_i}^2}\right) \quad (2)$$

$$J_{SC} = qG(L_n + L_p) \quad (3)$$

where $(kT)/q$ is the thermal voltage, $N_{D,A}$ is the donor or acceptor concentration of the wafer, Δn is the excess carrier concentration, n_i is the intrinsic carrier concentration, q is the magnitude of the electrical charge on the electron, G is the generation rate, and L_n and L_p are electron and hole diffusion lengths, respectively. Although the equations are based on several assumptions, one can see that V_{OC} and J_{SC} depend strongly on excess carrier concentration and diffusion length, which are directly proportional to the τ_{eff}. Accordingly, the increase in V_{OC} and J_{SC} due to improved τ_{eff} gives rise to the power conversion efficiency of 15.2% for the SHJ solar cell with hierarchical structures, showing the feasibility of hierarchical structures consisting of grooves and pyramids in solar cell applications. Furthermore, as displayed in Figure 5c, the substantial increase in external quantum efficiency (EQE) from 300 to 1100 nm shows that the broadband light-trapping characteristics of hierarchical structures could readily contribute to the J_{SC} enhancement. To show the accuracy of EQE measurements, we compared integrated J_{SC} from EQE measurements and J_{SC} from $J-V$ measurements, as discussed and indicated in Table S2 in the Supporting Information.

Moreover, according to eq 2, the implied V_{OC} can be obtained from Δn (which is related to τ_{eff}), assuming no electrical losses in subsequent layers (intrinsic, n-type, and p-type a-Si:H, ITO, and Ag) and contacts (between these electrodes and layers). From Table S3 in the Supporting Information, the mismatch between implied V_{OC} and realistic V_{OC} of SHJ solar cells indicates that V_{OC} can be further improved by optimizing the cell fabrication process for boosting the efficiency of cells with hierarchical structures, which is under investigation.

To demonstrate that microscaled hierarchical structures exhibit higher potential for PV performances than nanostructures, we fabricated the SHJ solar cell with nanoscaled hierarchical structures (*i.e.*, hierarchical structures combining micropyramids and NWs) for a comparison. SEM images, reflectance spectra, and PV characteristics of SHJ solar cells with nanoscaled and microscaled hierarchical structures are compared in Figure S4a–c and Table S4 in the Supporting Information. Note that for fairly examining nanoscaled hierarchical structures, we fabricated NWs on micropyramidal surfaces with a variety of lengths using metal-assisted chemical etching,[40] and only the PV performance of nanoscaled hierarchical SHJ cells with the optimized NW length is shown here. In Figure S4b, the substrates with nanoscaled hierarchical structures show much better AR property than the substrates with microscaled hierarchical structures due to the gradient refractive index effect of NWs, allowing more photons to enter the devices. Moreover, to emphasize the difference in p–n junction areas between two kinds of hierarchical structures, we define the roughness factor (RF) as the actual surface area of the structures divided by the projected area. The RF values of two different scaled hierarchical structures are estimated from SEM images (Figure 1 and Figure S4 in the Supporting Information). Theoretically, a higher RF provides more p–n junction areas, promotes more photocarriers being effectively separated, and then increases the J_{SC}.[41–43] The RF of nanoscaled hierarchical structures (20.67) is 11.17 times higher than that of microscaled hierarchical structures (1.85). However,

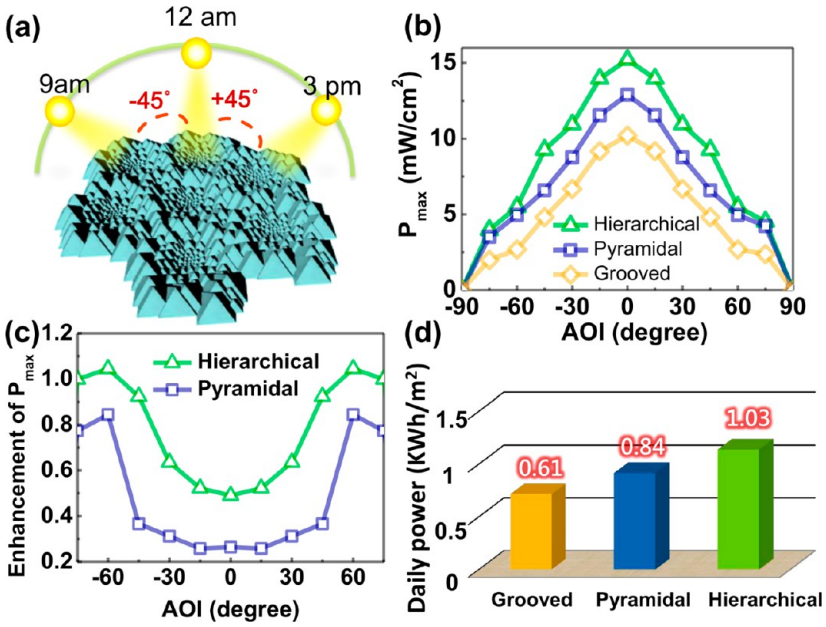

Figure 6. (a) Schematic of incident angle-dependent power generation over a day, (b) AOI dependence of generated maximum power, (c) enhancement of generated maximum power, and (d) estimated average daily power density generated from the devices with three kinds of surface structures.

the solar characteristics of nanoscaled hierarchical structures are much worse than those of microscaled hierarchical structures even though nanoscaled hierarchical structures exhibit superior light-trapping characteristics and much larger p−n junction areas.

This superior PV performance of microscaled hierarchical structures could be attributed to (i) less surface defect density and (ii) strong scattering effect. As shown in Figure S4d in the Supporting Information, the minority carrier lifetime of microscaled hierarchical structures is much higher than that of nanoscaled hierarchical structures due to the high-density surface defects of nanostructures. The photocarrier collection efficiency mainly depends on the minority carrier lifetime. Despite excellent AR characteristics and ultrahigh p−n junction areas, poor PV performance would still be obtained if photocarriers cannot be successfully extracted. Furthermore, the small feature size (*e.g.*, < 100 nm) of nanoscaled hierarchical structures is not thoroughly beneficial for light absorption, although the reflectance is vastly eliminated by nanostructured surfaces of nanoscaled hierarchical structures.[44,45] This is because, as the feature size is too small, light with relatively long wavelengths cannot resolve the structure geometries and thus the optical diffraction is weak, giving rise to straight propagation of the incident light through the medium. This leads to the fact that the optical thickness would be almost equal to the actual thickness, resulting in the ambiguous improvement of light absorption. In contrast, after the light strikes microscaled hierarchical structures, the structures scatter the light with large scattering angles to increase the duration of light staying in the active layer to enhance the effective optical thickness and then enhance the absorption in a wide range of wavelengths. Consequently, by combining superior electrical properties (by improving τ_{eff}) and effective light-trapping effect (by enhancing light scattering) of the microscaled hierarchical structures, excellent PV performance of microscaled hierarchical structures can be obtained.

All of PV characterizations discussed above were performed with normal incident light. However, the conversion of light into electric energy occurring at a wide range of AOIs should be considered for practical PV applications. As displayed in Figure 6a,b, the AOI-dependent maximum power density (P_{max} = $J_{SC}\cdot V_{OC}\cdot$FF) measurement was carried out under AM 1.5G illumination from −90° to 90° to characterize the omnidirectional light-trapping ability of three kinds of structures. It can be seen that generally the power density decreases as the striking angle increases. To clearly observe the relation of AOI-dependent P_{max} between grooved, pyramidal, and hierarchical structures, we define the P_{max} enhancement as $(P_{max,structured} - P_{max,groove})/P_{max,groove}$, where $P_{max,groove}$ and $P_{max,structured}$ are the P_{max} of groove and structured (pyramidal or hierarchical) devices, respectively. As shown in Figure 6c, compared to cells with grooved surfaces, cells with pyramidal surfaces show only a slight increase in the P_{max} enhancement as the AOI increases from 0° to ±75°, indicating that the light-trapping ability at high AOIs for grooved and pyramidal surfaces is similar. However, for cells with hierarchical structures, the P_{max} enhancement is increased from 49% to 104% as the AOI increases from 0° to 60°, implying that the

light-harvesting capability for cells with hierarchical structures is pronounced particularly at high AOIs. As shown in Figure 6d, we performed the day-integrated solar energy generation analysis, in which we assume that (i) the device and the sun are confined within the equatorial plane and (ii) the integrated P_{max} at the AOI from −90° to +90° represents the average daily power density generated from the solar cells. Cells with hierarchical structures exhibit a daily power density enhancement of 69%, as compared to cells with grooved surfaces. The daily power density enhancement (69%) higher than the power density enhancement at normal AOI (49%) for cells with hierarchical structures indicates that omnidirectional light-trapping characteristics of the hierarchical structure are beneficial for harvesting solar energy during a day without applying additional solar tracking systems. This also suggests that SHJ cells with hierarchical structures are capable of working on a hazy day.

CONCLUSION

In summary, hierarchical structures composed of grooves and pyramids in different scales exhibit favorable omnidirectional broadband light-trapping ability. The pyramids arranged at different heights on the grooved surfaces provide more bounces for the incoming light and exhibit strong light scattering, further improving the AR characteristics and enhancing light absorption characteristics. The excellent photon management of microscaled hierarchical structures allows the shrinkage of device thickness, improving the carrier lifetime and then achieving high *J*sc, *V*oc, and FF simultaneously. The SHJ solar cell fabricated with hierarchical structures using as-cut CZ n-type Si substrates displays excellent PV performance with an efficiency of 15.2%, a V_{OC} of 607 mV, and a J_{SC} of 36.4 mA/cm^2. The enhancement of generated power density at the AOI of 60° (104%) higher than that at normal AOI (49%) results in higher daily power density generated in hierarchical-structured SHJ cells (1.03 kWh/m^2, compared with 0.61 kWh/m^2 for grooves and 0.84 kWh/m^2 for pyramids), demonstrating the prominent omnidirectional operation ability. The achievement of high-efficiency omnidirectional solar cells using as-cut CZ n-type substrates demonstrated here makes the hierarchy concept highly attractive for large-area and cost-effective solar production.

EXPERIMENTAL SECTION

As-cut monocrystalline n-type CZ (100) Si wafers with a resistivity of 5−10 Ω-cm were used in this study. Surface structures of Si substrates were prepared by employing isotropic and anisotropic wet etching treatments. Before surface texturing, the samples were dipped into HF solution to remove the native oxide and then rinsed with deionized water.

After the wet etching processes, all samples were cleaned by standard RCA cleaning processes followed by 1% HF dipping. The plasma-enhanced chemical vapor deposition process was used for the deposition of intrinsic/p-type a-Si:H on the front and intrinsic/n-type a-Si:H layer on the rear. For the contact metal, ITO contacts were deposited by sputtering, followed by Ag grids on the front and a full coverage of Ag on the rear using e-gun evaporation.

The surface morphology was observed using a JEOL JSM-6700f field-emission scanning electron microscope. The R_{total} spectra were measured by a standard UV−vis spectrometer (JASCO ARN-733) with an integrating sphere. The distribution of electromagnetic fields within three kinds of surfaces was simulated based on FDTD analysis. After thin a-Si:H layers were deposited on both sides of monocrystalline Si, the effective carrier recombination was analyzed by minority carrier lifetime using the quasi-steady-state photoconductance technique with Sinton WCT120. The *J*−*V* measurements of the SHJ solar cells under the illumination of AM 1.5G were carried out with a Keithley 4200 source meter. The EQE measurements were performed by coupling the halogen lamp to a monochromator.

Conflict of Interest: The authors declare no competing financial interest.

Acknowledgment. This work was supported in part by the National Science Council of Taiwan under 102-2628-M-002-006-MY3, 101-2221-E-002-115-MY2, 101-2218-E-007-009-MY3, and 102-2633-M-007-002 and in part by the National Taiwan University (10R70823) and National Tsing Hua University through grant no. 102N2022E1. Y.L.C. greatly appreciates the use of the facility at CNMM, National Tsing Hua University, through grant no. 102N2744E1.

Supporting Information Available: Photovoltaic characteristics of n-type Si solar cells with photon management by structuring Si substrates; cross-sectional SEM images of grooved, pyramidal, and hierarchical structures; finite-difference time domain simulation; and comparison of integrated JSC from EQE measurements and JSC from *J*−*V* measurements. These materials are available free of charge *via* the Internet at http://pubs.acs.org.

REFERENCES AND NOTES

1. Zhu, J.; Yu, Z.; Fan, S.; Cui, Y. Nanostructured Photon Management for High Performance Solar Cells. *Mater. Sci. Eng. Rep.* **2010**, *70*, 330–340.
2. Chao, Y. C.; Chen, C. Y.; Lin, C. A.; Dai, Y. A.; He, J. H. Antireflection Effect of ZnO Nanorod Arrays. *J. Mater. Chem.* **2010**, *20*, 8134–8138.
3. Dai, Y. A.; Chang, H. C.; Lai, K. Y.; Lin, C. A.; Chung, R. J.; Lin, G. R.; He, J. H. Subwavelength Si Nanowire Arrays for Self-Cleaning Antireflection Coatings. *J. Mater. Chem.* **2010**, *20*, 10924–10930.
4. Lin, Y. R.; Wang, H. P.; Lin, C. A.; He, J. H. Surface Profile-Controlled Close-Packed Si Nanorod Arrays for Self-Cleaning Antireflection Coatings. *J. Appl. Phys.* **2009**, *106*, 114310.
5. Wei, W. R.; Tsai, M. L.; Ho, S. T.; Tai, S. H.; Ho, C. R.; Tsai, S. H.; Liu, C. W.; Chung, R. J.; He, J. H. Above-11%-Efficiency Organic-Inorganic Hybrid Solar Cells with Omnidirectional Harvesting Characteristics by Employing Hierarchical Photon Trapping Structures. *Nano Lett.* **2013**, *13*, 3658–3663.
6. Kelzenberg, M. D.; Boettcher, S. W.; Petykiewicz, J. A.; Turner-Evans, D. B.; Putnam, M. C.; Warren, E. L.; Spurgeon, J. M.; Briggs, R. M.; Lewis, N. S.; Atwater, H. A. Enhanced Absorption and Carrier Collection in Si Wire Arrays for Photovoltaic Applications. *Nat. Mater.* **2010**, *9*, 239–244.
7. Fan, Z.; Ruebusch, D. J.; Rathore, A. A.; Kapadia, R.; Ergen, O.; Leu, P. W.; Javey, A. Challenges and Prospects of Nanopillar-Based Solar Cells. *Nano Res.* **2009**, *2*, 829–843.

8. Lin, C. A.; Huang, K. P.; Ho, S. T.; Huang, M. W.; He, J. H. An Energy-Harvesting Scheme Utilizing Ga-Rich $CuIn_{(1-X)}Ga_XSe_2$ Quantum Dots for Dye-Sensitized Solar Cells. *Appl. Phys. Lett.* **2012**, *101*, 123901–123901−4.
9. Ho, C. H.; Lien, D. H.; Hsiao, Y. H.; Tsai, M. S.; Chang, D.; Lai, K. Y.; Sun, C. C.; He, J. H. Enhanced Light-Extraction from Hierarchical Surfaces Consisting of p-GaN Microdomes and SiO_2 Nanorods for GaN-Based Light-Emitting Diodes. *Appl. Phys. Lett.* **2013**, *103*, 161104.
10. Yeh, L. K.; Lai, K. Y.; Lin, G. J.; Fu, P. H.; Chang, H. C.; Lin, C. A.; He, J. H. Giant Efficiency Enhancement of GaAs Solar Cells with Graded Antireflection Layers Based on Syringelike ZnO Nanorod Arrays. *Adv. Energy Mater.* **2011**, *1*, 506–510.
11. Hsu, C. Y.; Lien, D. H.; Lu, S. Y.; Chen, C. Y.; Kang, C. F.; Chueh, Y. L.; Hsu, W. K.; He, J. H. Supersensitive, Ultrafast, and Broad-Band Light-Harvesting Scheme Employing Carbon Nanotube/TiO_2 Core-Shell Nanowire Geometry. *ACS Nano* **2012**, *6*, 6687–6692.
12. Wang, H. P.; Lin, T. Y.; Hsu, C. W.; Tsai, M. L.; Huang, C. H.; Wei, W. R.; Huang, M. Y.; Chien, Y. J.; Yang, P. C.; Liu, C. W.; *et al*. Realizing High-Efficiency Omnidirectional n-Type Si Solar Cells *via* the Hierarchical Architecture Concept with Radial Junctions. *ACS Nano* **2013**, *7*, 9325–9335.
13. Ho, C. H.; Lien, D. H.; Chang, H. C.; Lin, C. A.; Kang, C. F.; Hsing, M. K.; Lai, K. Y.; He, J. H. Hierarchical Structures Consisting of SiO_2 Nanorods and p-GaN Microdomes for Efficiently Harvesting Solar Energy for InGaN Quantum Well Photovoltaic Cells. *Nanoscale* **2012**, *4*, 7346–7349.
14. Lin, C. A.; Lai, K. Y.; Lien, W. C.; He, J. H. An Efficient Broadband and Omnidirectional Light-Harvesting Scheme Employing a Hierarchical Structure Based on a ZnO Nanorod/Si_3N_4-Coated Si Microgroove on 5-Inch Single Crystalline Si Solar Cells. *Nanoscale* **2012**, *4*, 6520–6526.
15. Zhang, Y. Y.; Zhang, J.; Luo, G.; Zhou, X.; Xie, G. Y.; Zhu, T.; Liu, Z. F. Fabrication of Silicon-Based Multilevel Nanostructures *via* Scanning Probe Oxidation and Anisotropic Wet Etching. *Nanotechnology* **2005**, *16*, 422–428.
16. Chang, H. C.; Lai, K. Y.; Dai, Y. A.; Wang, H. H.; Lin, C. A.; He, J. H. Nanowire Arrays with Controlled Structure Profiles for Maximizing Optical Collection Efficiency. *Energy Environ. Sci.* **2011**, *4*, 2863–2869.
17. Wang, H. P.; Lai, K. Y.; Lin, Y. R.; Lin, C. A.; He, J. H. Periodic Si Nanopillar Arrays Fabricated by Colloidal Lithography and Catalytic Etching for Broadband and Omnidirectional Elimination of Fresnel Reflection. *Langmuir* **2010**, *26*, 12855–12858.
18. Kuo, S.-Y.; Hsieh, M.-Y.; Han, H.-V.; Lai, F.-I.; Tsai, Y.-L.; Yang, J.-F.; Chuang, T.-Y.; Kuo, H.-C. Dandelion-Shaped Nanostructures for Enhancing Omnidirectional Photovoltaic Performance. *Nanoscale* **2013**, *5*, 4270–4276.
19. Oh, S. J.; Chhajed, S.; Poxson, D. J.; Cho, J.; Schubert, E. F.; Tark, S. J.; Kim, D.; Kim, J. K. Enhanced Broadband and Omni-Directional Performance of Polycrystalline Si Solar Cells by Using Discrete Multilayer Antireflection Coatings. *Opt. Express* **2012**, *21*, A157–A166.
20. Yan, X.; Poxson, D. J.; Cho, J.; Welser, R. E.; Sood, A. K.; Kim, J. K.; Schubert, E. F. Enhanced Omnidirectional Photovoltaic Performance of Solar Cells Using Multiple-Discrete-Layer Tailored- and Low-Refractive Index Anti-Reflection Coatings. *Adv. Funct. Mater.* **2013**, *23*, 583–590.
21. Peng, K.-Q.; Wang, X.; Wu, X.-L.; Lee, S.-T. Platinum Nanoparticle Decorated Silicon Nanowires for Efficient Solar Energy Conversion. *Nano Lett.* **2009**, *9*, 3704–3709.
22. Glunz, S.; Rein, S.; Lee, J.; Warta, W. Minority Carrier Lifetime Degradation in Boron-Doped Czochralski Silicon. *J. Appl. Phys.* **2001**, *90*, 2397–2404.
23. Macdonald, D.; Geerligs, L. J. Recombination Activity of Interstitial Iron and Other Transition Metal Point Defects in p- and n-Type Crystalline Silicon. *Appl. Phys. Lett.* **2004**, *85*, 4061–4063.
24. Kazmerski, L. L. Photovoltaics: A Review of Cell and Module Technologies. *Renewable Sustainable Energy Rev.* **1997**, *1*, 71–170.
25. Cheng, Y.-T.; Ho, J.-J.; Tsai, S.-Y.; Ye, Z.-Z.; Lee, W.; Hwang, D.-S.; Chang, S.-H.; Chang, C.-C.; Wang, K. L. Efficiency Improved by Acid Texturization for Multi-Crystalline Silicon Solar Cells. *Sol. Energy* **2011**, *85*, 87–94.
26. Chung, H.-Y.; Chen, C.-H.; Chu, H.-S. Analysis of Pyramidal Surface Texturization of Silicon Solar Cells by Molecular Dynamics Simulations. *Int. J. Photoenergy* **2008**, *2008*, 282791–282791−6.
27. Lien, S.-Y.; Yang, C.-H.; Hsu, C.-H.; Lin, Y.-S.; Wang, C.-C.; Wuu, D.-S. Optimization of Textured Structure on Crystalline Silicon Wafer for Heterojunction Solar Cell. *Mater. Chem. Phys.* **2012**, *133*, 63–68.
28. Park, H.; Kwon, S.; Lee, J. S.; Lim, H. J.; Yoon, S.; Kim, D. Improvement on Surface Texturing of Single Crystalline Silicon for Solar Sells by Saw-Damage Etching Using an Acidic Solution. *Sol. Energy Mater. Sol. Cells* **2009**, *93*, 1773–1778.
29. Nishimoto, Y.; Ishihara, T.; Namba, K. Investigation of Acidic Texturization for Multicrystalline Silicon Solar Cells. *J. Electrochem. Soc.* **1999**, *146*, 457–461.
30. Edwards, M.; Bowden, S.; Das, U.; Burrows, M. Effect of Texturing and Surface Preparation on Lifetime and Cell Performance in Heterojunction Silicon Solar Cells. *Sol. Energy Mater. Sol. Cells* **2008**, *92*, 1373–1377.
31. Neuwald, U.; Hessel, H. E.; Feltz, A.; Memmert, U.; Behm, R. J. Wet Chemical Etching of Si(100) Surfaces in Concentrated NH_4F Solution: Formation of (2 × 1)H Reconstructed Si(100) Terraces *versus* (111) Facetting. *Surf. Sci.* **1993**, *296*, L8–L14.
32. Angermann, H.; Henrion, W.; Röseler, A.; Rebien, M. Wet-Chemical Passivation of Si(111)- and Si(100)-Substrates. *Mater. Sci. Eng., B* **2000**, *73*, 178–183.
33. Burrows, M. Z.; Das, U. K.; Opila, R. L.; De Wolf, S.; Birkmire, R. W. Role of Hydrogen Bonding Environment in a-Si:H Films for c-Si Surface Passivation. *J. Vac. Sci. Technol., A* **2008**, *26*, 683–687.
34. Levi, D. H.; Teplin, C. W.; Iwaniczko, E.; Yan, Y.; Wang, T. H.; Branz, H. M. Real-Time Spectroscopic Ellipsometry Studies of the Growth of Amorphous and Epitaxial Silicon for Photovoltaic Applications. *J. Vac. Sci. Technol., A* **2006**, *24*, 1676–1683.
35. Sinton, R. A.; Cuevas, A. Contactless Determination of Current-Voltage Characteristics and Minority-Carrier Lifetimes in Semiconductors from Quasi-Steady-State Photoconductance Data. *Appl. Phys. Lett.* **1996**, *69*, 2510–2512.
36. Mishima, T.; Taguchi, M.; Sakata, H.; Maruyama, E. Development Status of High-Efficiency HIT Solar Cells. *Sol. Energy Mater. Sol. Cell* **2011**, *95*, 18–21.
37. McIntosh, K. R.; Cudzinovic, M. J.; Smith, D. D.; Mulligan, W. P.; Swanson, R. M. The Choice of Silicon Wafer for the Production of Low-Cost Rear-Contact Solar Cells. In *Proceedings of the 3rd World Conference on Photovoltaic Energy Conversion*; WCPEC-3 Organizing Committee: Osaka, Japan, 2003; 1, pp 971−974.
38. Fujishima, D.; Inoue, H.; Tsunomura, Y.; Asaumi, T.; Taira, S.; Kinoshita, T.; Taguchi, M.; Sakata, H.; Maruyama, E. High-Performance HIT Solar Cells for Thinner Silicon Wafers. In *Photovoltaic Specialists Conference. IEEE. 35th 2010*; IEEE, 2010; pp 003137−003140.
39. Taguchi, M.; Kawamoto, K.; Tsuge, S.; Baba, T.; Sakata, H.; Morizane, M.; Uchihashi, K.; Nakamura, N.; Kiyama, S.; Oota, O. HIT^{TM} Cells-High-Efficiency Crystalline Si Cells with Novel Structure. *Prog. Photovolt: Res. Appl.* **2000**, *8*, 503–513.
40. Wang, H. P.; Tsai, K. T.; Lai, K. Y.; Wei, T. C.; Wang, Y. L.; He, J. H. Periodic Si Nanopillar Arrays by Anodic Aluminum Oxide Template and Catalytic Etching for Broadband and Omnidirectional Light Harvesting. *Opt. Express* **2012**, *20*, A94–A103.
41. Dong, Z.; Lai, X.; Halpert, J. E.; Yang, N.; Yi, L.; Zhai, J.; Wang, D.; Tang, Z.; Jiang, L. Accurate Control of Multishelled ZnO Hollow Microspheres for Dye-Sensitized Solar Cells with High Efficiency. *Adv. Mater.* **2012**, *24*, 1046–1049.
42. Du, J.; Qi, J.; Wang, D.; Tang, Z. Facile Synthesis of Au@TiO_2 Core-Shell Hollow Spheres for Dye-Sensitized Solar Cells with Remarkably Improved Efficiency. *Energy Environ. Sci.* **2012**, *5*, 6914–6918.

43. Gao, Y.; Tang, Z. Design and Application of Inorganic Nanoparticle Superstructures: Current Status and Future Challenges. *Small* **2011**, *7*, 2133–2146.
44. Sai, H.; Fujiwara, H.; Kondo, M. Back Surface Reflectors with Periodic Textures Fabricated by Self-Ordering Process for Light Trapping in Thin-Film Microcrystalline Silicon Solar Cells. *Sol. Energy Mater. Sol. Cells* **2009**, *93*, 1087–1090.
45. Han, S. E.; Chen, G. Toward the Lambertian Limit of Light Trapping in Thin Nanostructured Silicon Solar Cells. *Nano Lett.* **2010**, *10*, 4692–4696.